ARTICLE

Wafer-Scale Patterning of Lead Telluride Nanowires: Structure, Characterization, and Electrical Properties

Yongan Yang, David K. Taggart, Matthew A. Brown, Chengxiang Xiang, Sheng-Chin Kung, Fan Yang, John C. Hemminger, and Reginald M. Penner*

Institute for Surface and Interface Science (ISIS), and the Department of Chemistry, University of California, Irvine, California 92697-2025

ABSTRACT Nanowires of lead telluride (PbTe) were patterned on glass surfaces using lithographically patterned nanowire electrodeposition (LPNE). LPNE involved the fabrication by photolithography of a contoured nickel nanoband that is recessed by ≈300 nm into a horizontal photoresist trench. Cubic PbTe was then electrodeposited from a basic aqueous solution containing Pb^{2+} and TeO_3^{2-} at the nickel nanoband using a cyclic deposition/stripping potential program in which lead-rich PbTe was first deposited in a negative-going potential scan and excess lead was then anodically stripped from the nascent nanowire by scanning in the positive direction to produce near stoichiometric PbTe. Repeating this scanning procedure permitted PbTe nanowires 60—400 nm in width to be obtained. The wire height was controlled over the range of 20—100 nm based upon the nickel film thickness. Nanowires with lengths exceeding 1 cm were prepared in this study. We report the characterization of these nanowires using X-ray diffraction, transmission electron microscopy and electron diffraction, scanning electron microscopy, and X-ray photoelectron spectroscopy (XPS). The surface chemical composition of PbTe nanowires was monitored by XPS as a function of time during the exposure of these nanowires to laboratory air. One to two monolayers of a mixed Pb and Te oxide are formed during a 24 h exposure. The electrical conductivity of PbTe nanowires was strongly affected by air oxidation, declining from an initial value of 2.0(±1.5) × 10^4 S/m by 61% (for nanowires with a 20 nm thickness), 55% (for 40 nm), and 12% (for 60 nm).

KEYWORDS: lead telluride · nanowire · electrodeposition · thermoelectric

PbTe, is a narrow band gap (E_g = 0.31 eV at 300 K) semiconductor material[1,2] that is among the most efficient materials known for thermoelectric power generation. In this application, PbTe is valued because of its excellent thermal stability which permits power generation at operating temperatures up to 1000 K.[3−6] The fraction of the Carnot efficiency ($\eta = T/T_h$) that is recoverable as power from a thermoelectric element is determined by its dimensionless figure-of-merit, ZT:[6]

$$ZT = \frac{\sigma T S^2}{\kappa} \quad (1)$$

where σ is the electrical conductivity of the thermoelement, S is its thermoelectric power or Seebeck coefficient, κ is its thermal conductivity, and T is the mean absolute temperature. PbTe has a ZT of 0.45 at 300 K and 0.85 at 700 K.[7]

Shrinking a conductor composed of thermoelectric material to the nanometer scale is predicted to increase S[8,9] and depress κ,[10−13] with both of these effects leading, *via* eq 1, to an elevation in ZT. Motivated by these predictions, tremendous effort has been devoted to the synthesis of PbTe nanomaterials.[14−25] Harman *et al.*[24,25] reported that the ZT at 300 K could be doubled from 0.45 to 0.9 for PbTe quantum dot superlattices and PbSeTe/PbTe quantum well superlattices prepared by molecular beam epitaxy (MBE). Their success has further stimulated experimental efforts to develop methods for synthesizing PbTe-based nanomaterials that, unlike MBE, are cheap and scalable.

Those non-MBE methods include chemical vapor transfer (CVT),[15] hydrothermal synthesis,[18] electrodeposition,[14,16,17,19] vacuum deposition,[26] and colloidal chemistry.[22] Using these methods, a diversity of PbTe nanomaterials has been prepared including films with nanometer-scale thickness,[16,17] nanoparticles,[22] nanocubes,[22] nanoflowers,[27] nanotubes,[19,20] nanorods,[28,29] and nanowires.[15,18,23,30,31] With regard to nanowires, the subject of the present paper, a number of methods have been developed. Yu *et al.*[18] reported that PbTe nanowires can be selectively synthesized by hydrothermal reaction of lead foil and tellurium powder using the reducing agent hydrazine and a surfactant. Yang *et al.*[15,23] developed a chemical vapor transfer (CVT) method for growing PbTe nanowires on silicon. Guo *et al.*[30,31] developed a hydrothermal method utilizing a Te nanowire as a template and $Pb(NO_3)_2$ as a precursor in concert with the reducing agent hydrazine. Liu *et al.*[14] reported the synthesis of single-crystalline PbTe nanowire arrays *via*

*Address correspondence to rmpenner@uci.edu.

Received for review September 7, 2009 and accepted November 18, 2009.

Published online December 1, 2009. 10.1021/nn901173p

electrodeposition using anodic aluminum oxide (AAO) membranes as templates. Ramanath *et al.*[28] developed a two-step template method in which Te nanotubes were first synthesized by solvothermal reduction of TeO_2 in the presence of surfactant followed by conversion into PbTe nanowires by exposure to $PbCl_2$ and hydrazine. All of these nanowire synthesis methods share one drawback: nanowires of PbTe are produced as free-standing objects within orientationally disordered powders. Additional processing steps must be carried out to position these nanowires on a surface and to establish electrical contacts in order to characterize the thermoelectric properties of these nanowires.

Here, we describe a method for patterning polycrystalline PbTe nanowires over wafer-scale areas on glass or silicon surfaces. This method is an adaptation of the lithographically patterned nanowire electrodeposition (LPNE) method that we have previously demonstrated for the preparation of metal nanowires on glass and silicon surfaces.[32−34] In LPNE, photolithography is used to pattern a nickel nanoband electrode that is recessed into a horizontal trench that is several hundred nanometers in width. This patterned electrode is then immersed into an aqueous synthesis solution, and the metal of interest is electroplated into this trench using the nickel nanoband as an electrode. Because the nanowire is formed by electrodeposition, a technique applicable to the deposition of a wide variety of materials, LPNE has tremendous versatility for the fabrication of nanowires having different compositions, but we have reported mainly on the fabrication of metal nanowires in our prior work.[32−36] Recently, we briefly described the application of LPNE to the preparation of suspended PbTe nanowires.[37] In this paper, we provide a complete description of the synthesis of PbTe nanowires using LPNE, we disclose data for the structural and compositional characterization of these nanowires, and we present the results of electrical conductivity measurements and a simultaneous X-ray photoelectron spectroscopy (XPS) investigation carried out as an oxide surface layer is formed in ambient air.

RESULTS AND DISCUSSION

The LPNE method involves the fabrication of a temporary sacrificial template on a glass or oxidized silicon surface (Figure 1).[32−34] This template is formed by first vapor depositing a nickel layer with a thickness of 5−100 nm, covering the nickel layer with a photoresist (PR) and photopatterning the PR layer, and then removing the exposed nickel using nitric acid. This nickel layer is intentionally "over etched" so that the PR layer is undercut by approximately 300−500 nm (Figure 1b) at the perimeter of the exposed region. This undercut produces a horizontal trench along the entire perimeter of the patterned region. A nanowire is formed within this trench by electrodeposition: the template is first immersed into an aqueous plating solution, and nanowires of the desired composition and width are produced by electrodeposition using the nickel edge within the trench as a working electrode. Finally, the template, consisting of the PR and nickel layers, is removed by dissolution in acetone and nitric acid, respectively, to expose the electrodeposited nanowires (Figure 1c). Useful features of the LPNE method include the following: (1) the position and two-dimensional trajectory of nanowires on the glass surface are controlled using photolithography; (2) the nanowire thicknesses, perpendicular to the surface, is determined by the thickness of the evaporated nickel layer; (3) the nanowire width is determined by the electrodeposition parameters (current, voltage, solution composition, and deposition time); and (4) electrical contacts to nanowires can be fabricated directly from the nickel layer, ensuring an intimate electrical contact to the nanowire and eliminating the influence of air oxidation on contact properties. We exploit this feature to make high-quality electrical contacts to PbTe nanowires in this paper.

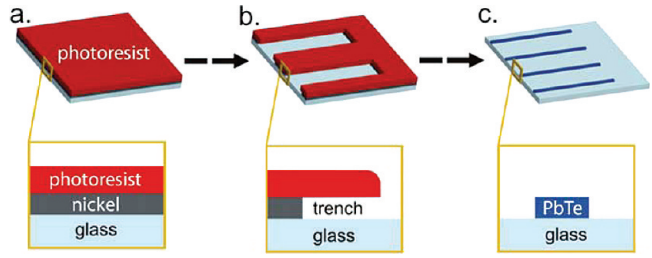

Figure 1. Synthesis of lead telluride nanowires using the LPNE method. Just three steps of the seven-step method are shown here. (a) Nickel layer is evaporated onto a glass surface (step 1) and covered with a layer of photoresist (PR, step 2). (b) PR layer is photopatterned using a contact mask (step 3), and the exposed nickel is etched in nitric acid to produce a horizontal trench along the perimeter of the exposed region (step 4). (c) PbTe nanowires are electrodeposited into this horizontal trench (step 5). The photoresist and remaining nickel are removed using acetone and nitric acid, respectively (steps 6 and 7).

Electrodeposition of PbTe. The electrodeposition of PbTe has been studied in some detail previously. Saloniemi *et al.*[16,17] studied the electrodeposition of PbTe on gold electrodes and proposed a deposition mechanism in which tellurium deposited first inducing the co-deposition of lead to form PbTe compound. A similar mechanism was also reported for the electrodeposition of Bi_2Te_3 by several groups.[38−43] In order to avoid the electrodeposition of excess tellurium, Saloniemi *et al.*[16,17] used a large stoichiometric excess (50:1) of lead in their plating solutions, but in spite of this, excess tellurium was detected in their electrodeposited PbTe films.[16,17] To mitigate this problem, we chose a concentration ratio of 100:1 (Pb/Te) for PbTe nanowire growth in this study (Figure 2).

The cyclic voltammetry (CV) of aqueous solutions containing just Te as TeO_3^{2-}, just Pb as Pb^{2+}, and both Pb and Te is shown in Figure 2. Our assignments of

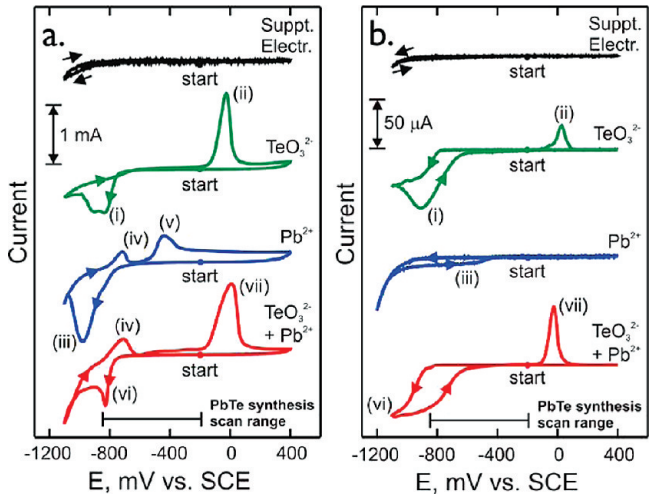

Figure 2. Cyclic voltammetry at 50 mV/s for three plating solutions at two electrodes: (a) an evaporated nickel film, (b) a patterned nickel nanoband prepared using the LPNE process. Black: supporting electrolyte (92 mM EDTA, 92 mM $NaNO_3$, pH = 10). Green: tellurium only (0.83 mM TeO_3^{2-}). Blue: lead only (83 mM Pb^{2+}). Red: both tellurium and lead (0.83 mM TeO_3^{2-}, 83 mM Pb^{2+}).

these peaks—based on both the prior work of Saloniemi *et al.* and our own EDX studies—are the following:[16,17]

peak (i) $TeO_3^{2-} + 6H^+ + 4e^- \rightarrow Te(s) + 3H_2O$

peak (ii) $Te(s) + 3H_2O \rightarrow TeO_3^{2-} + 6H^+ + 4e^-$

peak (iii) $Pb^{2+} + 2e^- \rightarrow Pb(s)$

peak (iv) $Pb(s) \rightarrow Pb^{2+} + 2e^-$

peak (v) $Pb(s) + H_2O \rightarrow PbO + 2H^+ + 2e^-$

peak (vi) $Pb^{2+} + TeO_3^{2-} + 3H_2O + 6e^- \rightarrow PbTe(s) + 6OH^-$ and reaction (iii)

peak (vii) $PbTe(s) + 6OH^- \rightarrow Pb^{2+} + TeO_3^{2-} + 3H_2O + 6e^-$

One immediately notices that the onset for PbTe deposition (Figure 2a,b, peak vi) coincides in potential with the onset of tellurium deposition (peak i), even though the onset for lead deposition occurs at a more negative potential, particularly at the nickel nanoband (Figure 2b, peak iii). This is evidence that the same mechanism proposed by Salenoemi *et al.*[16,17] operates here.

It is also apparent that, in solutions containing both TeO_3^{2-} and Pb^{2+}, cathodic electrodeposition at potentials negative of −600 mV *vs* SCE can produce elemental Pb (peak iii) and Te (peak i) in addition to PbTe, making the electrodeposition of stoichiometric PbTe difficult. Sailor and co-workers demonstrated an elegant solution to this problem in 1991[44] when they showed that near stoichiometric cadmium selenide could be electrodeposited using a cyclic electrodeposition−stripping method from solutions containing a 10-fold excess of Cd^{2+} relative to SeO_3^{2-}. In their experiment, elemental cadmium was electrodeposited together with CdSe on the negative-going synthesis scan, and excess cadmium was removed from the electrodeposit on the subsequent positive-going stripping scan.[44] Elemental selenium was not deposited because the growth of CdSe occurred at a rate that was diffusion-controlled by SeO_3^{2-}. We have successfully applied this electrodeposition/stripping strategy to the synthesis of nanowires composed of CdSe,[45] Bi_2Te_3,[38,46] and, recently, PbTe.[37]

For plating solutions containing both Pb^{2+} (83 mM) and TeO_3^{2-} (0.83 mM), a reduction peak is observed at −0.83 V (Figure 2, peak vi) that is assigned to the electrodeposition of PbTe compound and excess lead.[16,17] Two oxidation waves are observed at −0.76 V (peak iv) and 0.01 V (peak vii) that are produced by lead oxidation and anodic PbTe dissolution, respectively. By using −0.85 and −0.20 V as voltage limits for the synthesis scans, as indicated in Figure 2, excess lead is removed from the nascent PbTe deposit while the stripping of PbTe (at 0.01 V) is avoided. The evidence of this fact is not implicit in the electrochemistry alone, but it is apparent based on a detailed chemical analysis of the deposited material by XPS, EDX, and X-ray diffraction presented below. Excess elemental tellurium is not removed by this procedure, however, because this Te stripping occurs at the same potential as PbTe dissolution, so it is important to ensure that no excess elemental tellurium is deposited in the negative-going scan to −0.85 V. This is why we used a 100:1 Pb/Te ratio for the deposition solution in the experiments described here.

The electrochemistry at the nickel film (Figure 2a) and the nickel nanoband electrodes (Figure 2b) are similar, but the shape of the voltammetric waves reflects the differing geometries of these two electrodes. At the nickel nanoband, limiting-current plateaus expected for the nanoband geometry are seen for lead deposition (Figure 2b, peak iii) and PbTe deposition (peak vi), although for reasons that are not clear, the deposition wave for elemental tellurium does not show the same limiting-current shape (peak i).[16,17] Surprisingly, the lead electrodeposition reaction (blue curves) at the nickel nanoband (Figure 2b) shows a large overpotential on the forward (negative-going) scan. On the reverse scan, lead deposition continues, producing a cathodic current plateau, up to −450 mV. One explanation for this behavior is the suppression of lead nucleation within the confined nickel nanoband. However, similar shifts in the overpotential for PbTe and Te deposition are not seen in the data of Figure 2. The final difference is that the PbTe nanowire synthesis scans (Figure 2b, peak vi) show

virtually no lead stripping wave, and this suggests that very little excess lead is present in the as-deposited PbTe film. Below, we discuss the structural and chemical characterization of the PbTe nanowires by X-ray diffraction (XRD), energy dispersive X-ray analysis (EDX), and selected area electron diffraction (SAED).

The CVs shown in Figure 2 were acquired at 50 mV/s, and it is useful to ask whether the quality of the electrodeposited PbTe or its grain size depends on this variable. To address this question, we synthesized six PbTe nanofilms using scan rates of 1, 25, 50, 100, 200, and 1000 mV/s and XRD patterns were obtained for each (Figure 3a). The diffraction patterns obtained from PbTe layers deposited at 1 to 200 mV/s (curve a−e) can all be assigned to cubic PbTe powder (JCPDS 38-1435), and no extra lines are seen in these patterns. We conclude that stoichiometric, single-phase PbTe nanowires are obtained within a wide potential scan rate range. However, when the scan rate was increased to 1000 mV/s, only elemental Te was detectable. We postulate that the conversion of Te to PbTe that occurs during the negative-going voltammetric scan does not have sufficient time to occur at 1000 mV/s and Te only is therefore observed. In addition, at scan rates from 25 to 200 mV/s, the (220) reflection is much stronger than (200), suggesting that the dominant growth direction is (220). The reason for this discrepancy in crystalline orientations lies in the difference of growth speeds for different facets, which originates from the facet-dependent surface free energy. However, our earlier analysis of PbTe nanowires prepared by LPNE[37] did not reveal the presence of (220) texturing.

Using the XRD patterns of Figure 3a, PbTe crystalline sizes were calculated using the Scherrer equation:[47]

$$D = 0.89\frac{\lambda}{B\cos\theta} \qquad (2)$$

where D is the crystal size, λ is the X-ray wavelength, B is the full width of the peak measured at half-height, and θ is the diffraction angle. For scan rates from 1 to 200 mV/s, D is virtually independent of the scan rate and in the range from 16 to 19 nm (Figure 3b).

Dimensional Control. As in the case of metal nanowires,[32−34] the LPNE method provides for independent control of PbTe nanowire width and height. The height dimension of these nanowires is most accurately measured using AFM (Figure 4). The height of

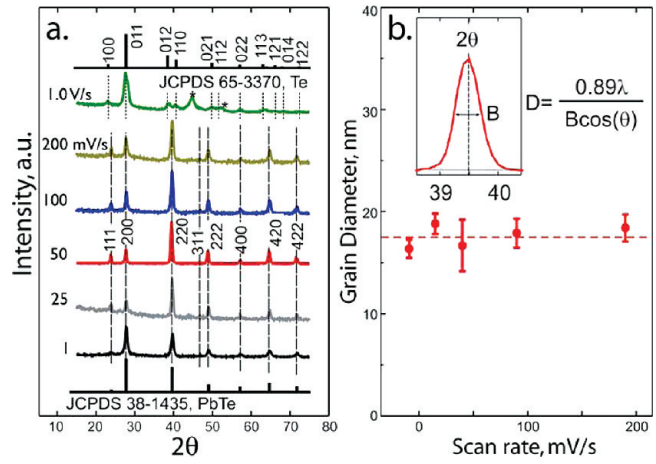

Figure 3. Effect of potential scan rate, from 1 mV/s (bottom) to 1 V/s (top), on the composition and grain size for electrodeposited PbTe films. (a) XRD patterns for PbTe layers ($t \approx 60$ nm) electrodeposited on nickel films using the cyclic electrodeposition/stripping method used for PbTe nanowire growth. The positive and negative limits for these scans were −0.2 V *vs* SCE and −0.85 V, respectively. Reference XRD stick patterns of fcc PbTe (JCPDS 38-1435, bottom) and hexagonal Te (JCPDS 65-3370, top) are shown. (b) Plot of mean grain diameter, *D*, *versus* potential scan rate for PbTe layers obtained by analysis of the patterns shown in (a) using the Scherrer equation.

PbTe nanowires prepared by LPNE equals the thickness of the nickel film evaporated in the first step of the fabrication process (Figure 4a).

Nanowire width is determined by the electrodeposition parameters, but in contrast to metals that are deposited potentiostatically,[32−34] PbTe nanowires were grown using the scanning electrodeposition/stripping

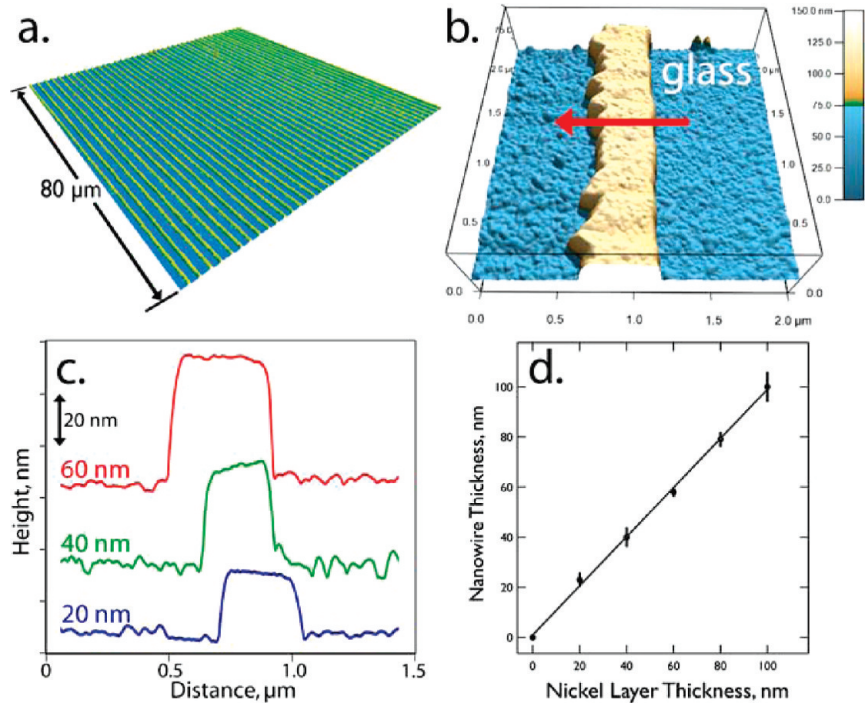

Figure 4. Atomic force micrographs at low magnification (a, 80 μm × 80 μm) and higher magnification (b, 2.0 μm × 2.0 μm) of PbTe nanowires. The red arrow indicates the growth direction. (c) Amplitude traces of three nanowires prepared using nickel films with the indicated heights of 20, 40, or 60 nm. (d) Plot of the mean height for PbTe nanwires as a function of the nickel layer thickness showing the linear dependence for five wire heights ranging from 20 to 100 nm.

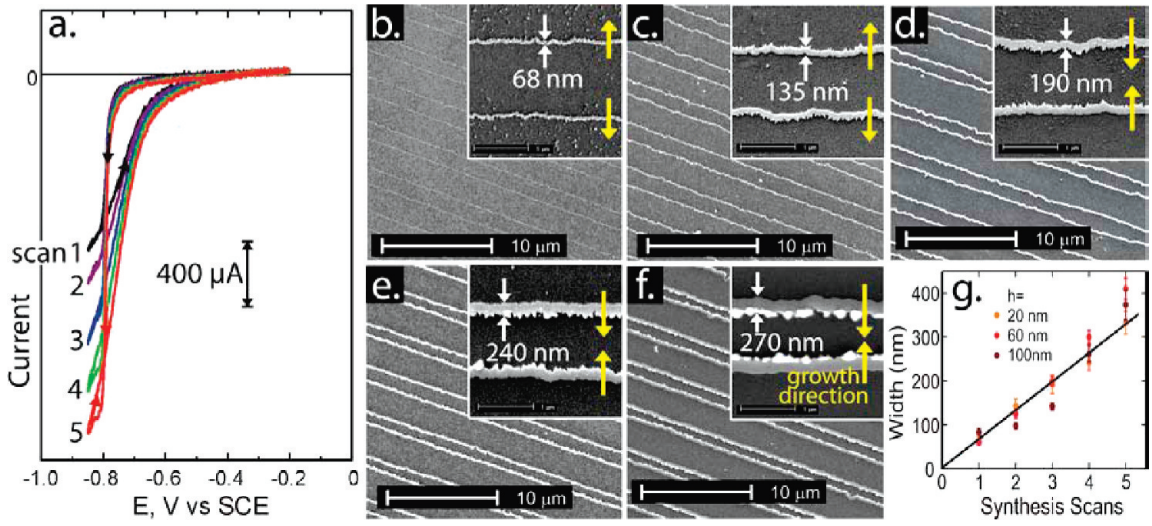

Figure 5. (a) Cyclic voltammograms (50 mV/s) for the synthesis of PbTe nanowires. The synthesis current increases with each successive scan as shown. (b−f) Scanning electron micrographs of PbTe nanowires at low magnification and higher magnification (inset). These nanowires were prepared using one synthesis scan (b), two synthesis scans (c), *etc*. Yellow arrows indicate the direction of nanowire growth. (g) Plot of mean wire width *versus* number of synthesis scans showing linear behavior for wires with heights of 20, 60, and 100 nm.

method. This means the wire width cannot be continuously varied. Instead, each deposition/stripping scan between −0.2 and −0.85 V adds 60−80 nm to the nanowire width. Five typical voltage scans are shown in Figure 5 together with SEMs of the PbTe nanowires obtained by depositing PbTe using 1−5 deposition scans. A closer examination of these nanowires (see Figure 5b−f, insets) reveals that one edge of the nanowire is rougher than the other. Invariably, the rougher of the two nanowire edges corresponds to solution-wetted edge of the nanowire, and the smoother edge is the edge that was in contact with the nickel film. Thus the growth direction is as indicated by the yellow arrows.

The arrays of parallel nanowires shown both in Figures 4 and 5 can cover a glass surface that is square inches in size—limited only by the size of the contact mask and the uniformity of the UV illumination used for patterning. Thus, this PbTe nanowire fabrication method is truly wafer scale.

Preparation of "Portable" PbTe Wire Arrays. We discovered by accident a method for preparing arrays of PbTe nanowires that are embedded in an ultrathin layer of photoresist. These "portable" PbTe nanowire arrays are

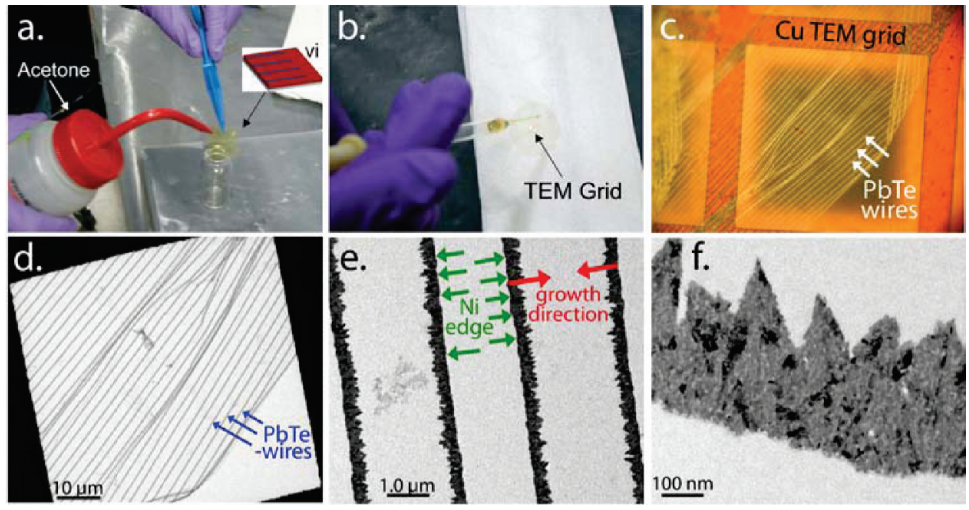

Figure 6. Portable PbTe nanowire arrays. (a,b) Arrays of PbTe nanowires may be transferred in an ultrathin photoresist layer from the glass surfaces on which they are synthesized to copper TEM grids. This process involves rinsing the nanowire-patterned, photoresist-covered glass with acetone (a) and then transferring the PR-entrained PbTe nanowires from the rinse catch vial using a Pasteur pipet onto a copper TEM grid (b). (c) Optical micrograph of a "portable" PbTe nanowire array. (d) Low-magnification TEM image of PbTe nanowires, (e,f) TEM images at higher magnification of PbTe nanowires that are 20 nm in thickness. Faceting of the solution-wetted nanowire edge is especially apparent for these 20 nm thick PbTe nanowires. The darkened areas seen within the nanowire in this image are individual PbTe grains.

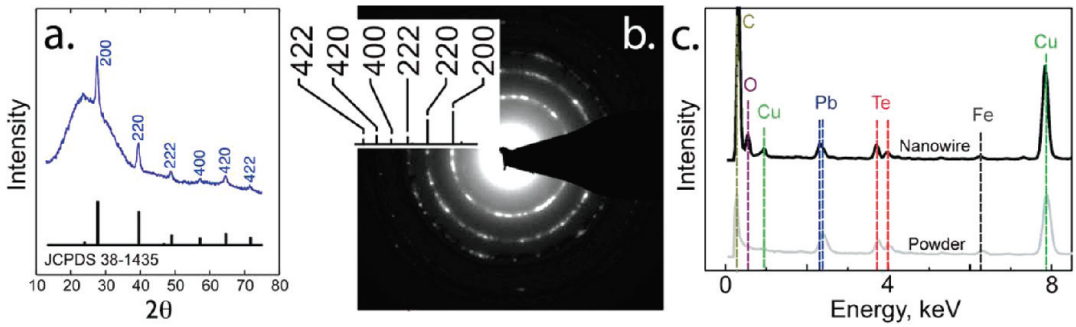

Figure 7. (a) Low-angle incidence X-ray diffraction (LIXRD) pattern for an array of PbTe nanowire arrays deposited at 2 μm pitch on glass. The broad peak centered at 25° derives from diffraction from the glass surface. (b) Selected area electron diffraction (SAED) analysis of the nanowire shown in Figure 6f. All reflections are assigned to cubic PbTe, JCPDS 38-1435. (c) Energy-dispersive X-ray analysis (EDX) carried out in transmission mode showing data for a single PbTe nanowire prepared by LPNE (red), and a sample of PbTe powder (Aldrich, 99.998%). Peaks assignable to C, O, Fe, and Cu are derived from either surface contamination or the TEM grid.

obtained by carrying out the LPNE process on a glass surface on which a photoresist layer (Shipley 1808) has first been spin-coated and "soft-baked". This photoresist-bottomed LPNE method is also employed to prepare suspended arrays of PbTe nanowires, as previously described.[37] Once PbTe nanowires are synthesized in the normal way on the photoresist surface, rinsing this surface with acetone removes arrays of the nanowires together with an ultrathin layer of photoresist (estimated to be less than 20 nm in thickness). This second acetone rinse releases PbTe nanowires by dissolving the "base layer" of photoresist supporting the nanowires on the glass surface. The outermost photoresist layer was removed, before removing the nickel electrode, by exposure to developer solution. Developer selectively removes just the outermost PR layer because it has been previously flood exposed. If the "runoff" from this second acetone rinse is captured using a vial (Figure 6a), intact nanowire arrays can be transferred by drawing this solution containing the suspended nanowire arrays into a Pasteur pipet and then delivering it to any surface (Figure 6b), including the surface of a TEM grid (Figure 6c). TEM (Figure 6e) images confirm that the individual PbTe nanowires in this portable array retain the same wire-to-wire pitch and orientation seen on a glass surface. In these bright field images, a subset of the PbTe grains in the nanowire appears dark because the crystallographic orientation of these grains matches the condition for diffraction and the electron beam is deflected off the detector instead of being transmitted. In high-magnification images (Figure 6f), these darkened grains show a mean diameter in the 10−20 nm range, approximately the same mean grain diameter obtained from XRD line broadening analysis (Figure 3). PbTe nanowires entrained within this photoresist film should have a high degree of thermal isolation, and these nanowire arrays may prove to be useful for future studies aimed at characterizing the thermal transport in these nanowires.

Low-angle incidence X-ray diffraction (LIXRD)[48,49] patterns acquired for arrays of PbTe nanowires deposited at 2 μm pitch (Figure 7a) and selected area electron diffraction patterns for individual nanowires (Figure 7b) can both be indexed to cubic PbTe (JCPDS 38-1435). Scherrer analysis of XRD line broadening yields a mean grain diameter in the 10−20 nm range, just as estimated by TEM and XRD of PbTe films (Figure 3). Energy-dispersive X-ray analysis (EDX) was carried out in transmission mode (Figure 7c). PbTe nanowires (red curve) were compared with commercial PbTe powder (Aldrich, 99.998%, blue curve). The intensity ratio, Pb/Te, obtained from these spectra for nanowires is 0.94, which is close to the value of 1.0 measured for the commercial PbTe powder. This result is consistent with a bulk composition for these nanowires that is close to stoichiometric.

X-ray Photoelectron Spectroscopy of PbTe Nanowires during Air Oxidation. X-ray photoelectron spectroscopy (XPS) was used to probe the surface chemical composition of PbTe nanowire arrays prepared by LPNE. The objectives of this study were to determine the chemical composition of the PbTe surface for freshly synthesized PbTe nanowires and to determine how the surface chemical composition evolves as a function of time during the exposure of these nanowires to laboratory air (Figure 8).

Deconvolution curve fitting was used to analyze the chemical states of the Pb and Te present at the nanowire surface. For Te(3d), two distinct chemical states are present in the spectra of Figure 8a. The spin−orbit splitting of each Te(3d) component gives rise to a doublet with energy separation of 10.4 eV.[50] The lower energy doublet with a binding energy (BE) for Te($3d_{5/2}$) of 572.9 eV (red) is assigned to PbTe.[52−54] The higher energy component with a Te($3d_{5/2}$) BE of 576.3 eV (purple) is assigned to TeO_2. Two distinct chemical states, again identified by a doublet of doublets, are also present in the spectra of Pb(4f). Each chemical state can be identified by a doublet corresponding to the spin−orbit splitting of the Pb(4f) orbital with an energy separation of 4.9 eV.[50] The lower energy component with a BE for Pb($4f_{7/2}$) of 137.3 eV

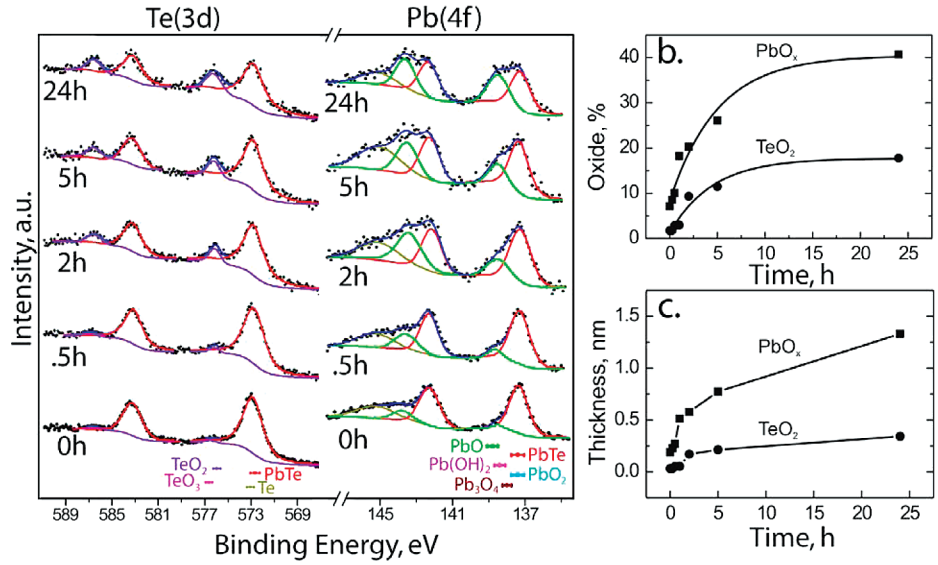

Figure 8. (a) X-ray photoelectron spectroscopy spectra of the Pb(4f) and Te(3d) regions acquired as a function of exposure time in laboratory air. Reference binding energies for various lead compounds and tellurium compounds are indicated at the bottom.[50] Te(3d) is deconvoluted into two components: PbTe (red) and TeO_2 (purple). The purple line also includes the Shirley background from the PbTe peak; Pb(4f) spectra are deconvoluted into four components: PbTe (red), PbO_x (green), Si(2p) in bronze, and the sum in dark blue. (b) Fraction of the total lead and tellurium present as PbO_x and TeO_2 plotted as a percentage *versus* the time of exposure to air. (c) Estimated thickness of the PbO_x and TeO_2 layers, calculated according to the Bando model,[51] plotted *versus* the time of exposure to air.

(red) is assigned to PbTe.[52−54] The higher energy component with a Pb($4f_{7/2}$) BE of 138.6 eV (green) is assigned to either $Pb(OH)_2$[52,55] or PbO.[56] A third, broad component at around 145 eV (bronze) is also seen in all Pb(4f) spectra. This peak is Si(2p) emission from the glass substrate.[50]

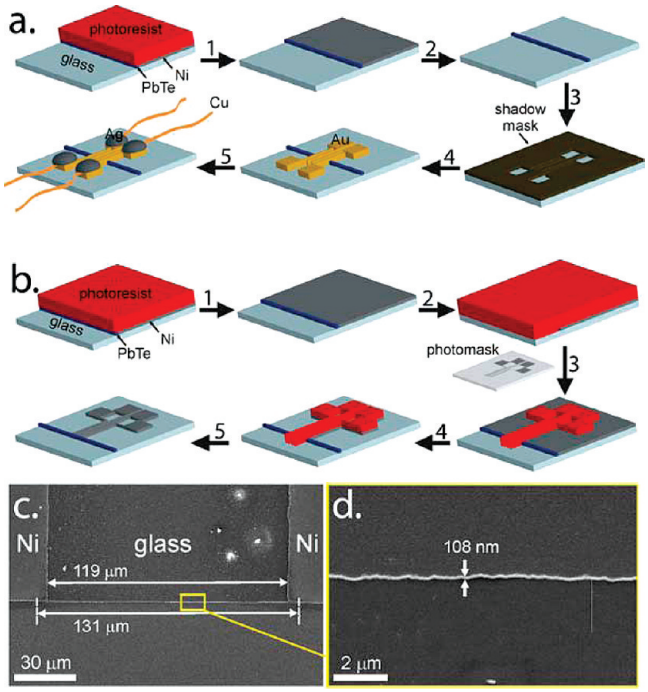

Figure 9. Making a single nanowire device for electrical conductivity measurements. (a) Four gold electrical contacts are evaporated *via* shadow mask onto the PbTe nanowire and then connected to copper wires through silver paste. *I*−*V* curve measurement can be performed after several hours drying. (b) Four nickel electrical contacts are fabricated from the evaporated nickel layer by carrying out a second photolithography patterning step. (c,d) SEM images of a PbTe nanowire with lithographically patterned nickel contacts at two magnifications.

Freshly prepared nanowires were rapidly transferred into the XPS chamber, experiencing less than 1 min of air exposure. Spectra for these nanowires, labeled "0h" in Figure 8, are dominated by doublets with chemical shifts consistent with PbTe.[52] These spectra permit the Pb/Te mole ratio to be estimated at 0.28: 1.0.[57] This is a surprisingly low Pb/Te ratio for the nanowire surface, especially considering the XRD data of Figures 3 and 7a, showing that these nanowires are single-phase PbTe. The underlying reason is unresolved, but two possible explanations are the following: (1) excess elemental Te in the bulk of the nanowire may migrate to the nanowire surface since it is known that, for metal chalcogenide nanocrystals, chalcogene terminatation is energetically favored relative to metal termination;[58] (2) PbO_x at the nanowire surface may be preferentially removed, relative to TeO_2, by the final nitric acid etch required for removal of the nickel sacrificial electrodes. It is important to note that the skewing of the Pb/Te ratio is not detected by EDX (Figure 7) because, for that technique, the probe depth far exceeds the thickness of our nanowires and the composition of the entire PbTe nanowire is probed. This is why the disparity between PbO_x and TeO_2 concentrations seen in Figure 8b,c can reasonably be attributed to preferential removal of PbO_x from the surface by nitric acid, and this conclusion does not conflict with the EDX result.

Smaller peaks for PbO_x and TeO_2 are already seen for the 0h sample, and the fraction of the total signals

for these oxide components are 7.2% for PbO_x and 1.8% for TeO_2 (Figure 8a,b). With continued exposure to air, PbO_x and TeO_2 peaks increased monotonically relative to the peaks for PbTe until, after 24 h, the PbO_x signal was 41% of the total for lead and TeO_2 was 18% of the total for tellurium. On the basis of the layered oxide structure model suggested by Bando *et al.*[48,51] and the inelastic mean free paths of the photoelectrons,[59] the equivalent thickness of oxide layers was estimated as a function of the air exposure duration (Figure 8c). After 24 h of air exposure, we estimate equivalent layer thicknesses of 1.3 nm for PbO_2 and 0.3 nm for TeO_2. In other words, PbO_2 grows faster than TeO_2 in spite of the fact that the surface of the PbTe nanowire is initially enriched in Te relative to Pb. The influence of this oxide overlayer on the electrical conductivity of these nanowires is examined next.

Electrical Conductivity Measurements during Air Oxidation. How does the oxidation of the PbTe nanowire surface in air affect its electrical conductivity? This is a critical issue from the standpoint of the thermoelectric performance of these nanowires because, as indicated by eq 1, the value of ZT for a material is directly proportional to its electrical conductivity, σ. We measured σ for single PbTe nanowires prepared by LPNE as a function of the exposure time to air. Especially because of the corrosive influence of air on the PbTe surface revealed by XPS (Figure 8), it is essential to preserve an intimate electrical contact to the nanowire during this experiment. For this reason, we abandoned the standard method for preparing electrical contacts[15,32,33] involving the evaporation of metal onto a nanowire that has already been exposed to air (Figure 9a). Our new method (Figure 9b) involves photolithographic patterning of the nickel film that is used for PbTe nanowire growth (Figure 9b). After PbTe nanowire growth, the initial photoresist is removed and a new layer of photoresist is spin-coated to fully cover the nanowire/nickel film (Figure 9b, step 2). The new photoresist layer is then photolithographically patterned using a four-probe photomask (step 3), and the exposed nickel film is removed with nitric acid (step 4). Finally, removal of the photoresist with acetone exposes the PbTe nanowire with four nickel contacts. The important point is that the PbTe surface where the nickel contacts are established is never exposed to air during this process.

Current *versus* voltage curves (Figure 10a) for single PbTe nanowires remain ohmic for the full 24 h air exposure, suggesting that the method outlined above (Figure 9b) prevents the formation of oxide at the electrical contact. When four nickel contacts are, instead, applied by vapor deposition to PbTe nanowires, the measured resistance values were a factor of 10 higher than measured using the method of Figure 10. The initial conductivity of these nanowires was in the range from 0.1×10^4 to 5.0×10^4 S/m, which coincides with the

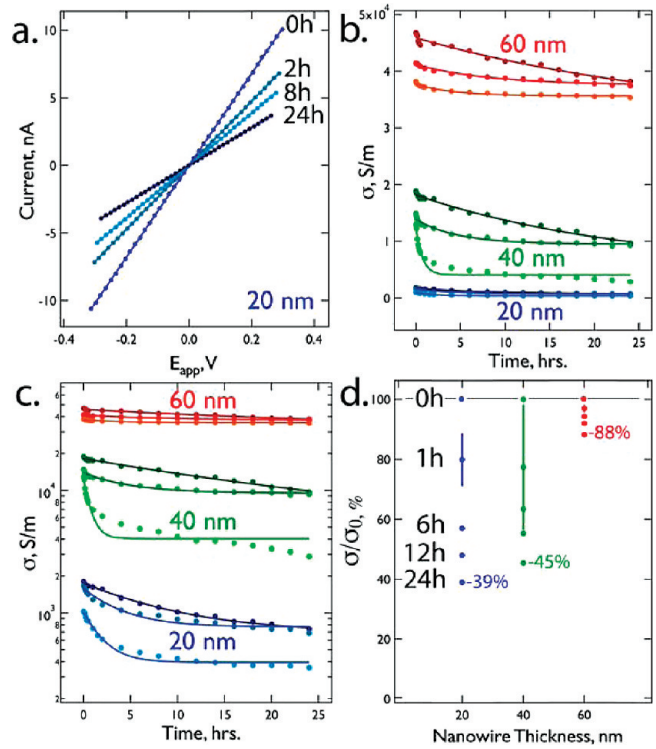

Figure 10. (a) Current *versus* voltage curves for a PbTe nanowire with dimensions of 20 nm × 108 nm × 123 μm during exposure to laboratory air. (b) Plot of the measured nanowire conductivity *versus* exposure time for nanowires of three thickness values: 20 nm (blue), 40 nm (green), and 60 nm (red). (c) Log−linear plot of the same data shown in (b) and (d). Plot of electrical conductivity (σ) normalized to time 0 against the nanowire thickness for five time points during the exposure to air.

range of conductivity values reported for PbTe films.[15,55,56] From this initial state, air exposure reduces the electrical conductivity of PbTe nanowires as the surface oxide is formed (Figure 10b−d). Electrical conductivity *versus* time data were acquired for nine nanowires, with thicknesses, t, of 20, 40, and 60 nm. These nanowires had similar widths, in the range from 100 to 150 nm. The fraction of the initial conductivity, σ_0, that was retained after a 24 h air exposure was 88% for $t = 60$ nm wires, 45% for $t = 40$ nm, and 39% for $t = 20$ nm nanowires. According to the XPS data of Figure 9, such nanowires have just 1.3 nm of oxide on their surfaces.

How can the presence of the ultrathin oxide layer measured by XPS be reconciled with the 60% loss in conductivity seen for the 20 nm PbTe nanowires? We can conceive of two possible explanations: First, the growth of the oxide layer could alter doping in the nanowire. It is well-established[55,60] that, in the case of n-type PbTe, oxygen acts as a p-type dopant increasing the hole concentration and eventually inverting the majority carrier type. For n-type PbTe, this mechanism leads initially to a loss in conductivity as n-type dopants are compensated. We note here that ongoing measurements of the Seebeck coefficient, S, reveal that freshly prepared PbTe nanowires are reproducibly n-type. A second contributing factor may be the penetration of oxide into the grain boundaries near the wire surface.

We have recently invoked this mechanism to account for the loss in conductivity of gold nanowires (up to 70%) induced by the formation of a single $Au(OH)_3$ monolayer.[35]

CONCLUSIONS

These data support the following conclusions:

1. The LPNE method can be adapted to produce single-phase, cubic PbTe nanowires on glass surfaces.
2. Growth of PbTe involves the electrodeposition of PbTe using a cyclic electrodeposition/stripping method in which lead-rich PbTe is first electrodeposited, and excess lead is then anodically stripped from the nascent nanowire. By skewing the mole ratio of Pb/Te strongly in favor of Pb (100:1), the electrodeposition of elemental Te is avoided during this process. Repeating this cyclic electrodeposition/stripping process allows near stoichiometric PbTe nanowires to be built up in 60−80 nm increments.
3. These PbTe nanowires have a rectangular cross section with height and width dimensions that are independently adjustable, down to minimum values of 20 and 70 nm, respectively.
4. These nanowires are polycrystalline with a mean grain diameter of 10−20 nm.
5. "Portable" nanowire arrays, consisting of PbTe nanowires entrained in an ultrathin photoresist layer, can be prepared by rinsing a photoresist-supported PbTe array with acetone. These arrays are suspended in the recovered wash solution, and they can be transferred (*e.g.*, onto a TEM grid) using a Pasteur pipet.
6. Wire surfaces are initially tellurium-rich, but oxidation in laboratory air more rapidly produces PbO_2 (1.3 nm in 24 h) relative to TeO_2 (0.3 nm in 24 h).
7. Commensurate with wire oxidation is a progressive loss in the electrical conductivity of PbTe nanowires of up to 60% for wires with a thickness of 20 nm. We hypothesize that this loss in conductivity derives from the progressive and compensative p-doping of initially n-type PbTe nanowires.

METHODS

Chemicals. Optical glass slides (1 in. × 1 in.) were purchased from Fisher and used as substrates. Nickel wire (Ni, 99.99%) and tellurium oxide (TeO_2, 99.9995%) were used as received from Aldrich. Positive photoresists S1808 and S1827 and developer F319 were purchased from Microchem. Lead nitrate ($Pb(NO_3)_2$, 99.4%, Certificated ACS), sodium nitrate ($NaNO_3$, 100.1%, certificated ACS), EDTA (disodium ethylenediaminetetraacetate, 99.8%), acetone (GR, ACS), and pH = 10 buffer solution were used as received from Fisher.

Plating Solution. EDTA (5.5 mmol) and $NaNO_3$ (5.5 mmol) were dissolved in 40 mL of buffer solution of pH = 10. Then 5 mmol of $Pb(NO_3)_2$ and 0.05 mmol of TeO_2 were added and dissolved while maintaining the pH at 10.0. The final volume of the solution was adjusted to 60 mL. The final concentrations of each component are 83 mM for $Pb(NO_3)_2$, 0.83 mM for TeO_2 (in the form of TeO_3^{2-}), 92 mM EDTA, and 92 mM $NaNO_3$.

TEM (Transmission Electron Miscroscopy) and SAED (Selected Area Electron Diffraction). TEM images and SAED were acquired using a Phillips CM 20 TEM using an accelerating voltage of 200 kV. PbTe nanowires, prepared on a photoresist-covered glass surface, were transferred to a glass vial in an ultrathin PR layer by rinsing the surface with acetone. These PbTe arrays were then drop-coated onto carbon-film-coated copper grids (Ted Pella) using a Pasteur pipet. These grids were then dried overnight before TEM measurements.

SEM (Scanning Electron Microscopy). Scanning electron microscopy (SEM) images were collected on Philips XL-30 FEGSEM (field emission gun scanning electron miscrocope) using an accelerating voltage of 10 kV. The samples were mounted on aluminum stubs (Ted Pella) using adhesive carbon tape.

XRD (X-ray Diffraction). LIXRD (low-angle incidence X-ray diffraction)[48,49] technique was employed to analyze the crystallinity of PbTe nanowires and nanofilm. A fixed low angle of incidence for the X-ray beam makes the analysis more sensitive to the sample surface and thus leads to higher diffraction intensities. LIXRD was performed using a Rigaku Ultima III (Rigaku, Tokyo, Japan) high-resolution X-ray diffractometer with Cu Kα irradiation and an incident angle of 0.6°.

XPS (X-ray Photoelectron Spectroscopy). XPS measurements were performed with an ESCALAB MKII (VG Scientific) surface analysis instrument. The ultrahigh vacuum multichamber system is equipped with a twin anode X-ray source (Mg/Al) and a 150 mm hemispherical electron energy analyzer. Spectra presented here were collected using Mg Kα X-rays (1253.6 eV) in constant energy mode with a pass energy of 20 eV. During acquisition, the base pressure of the spectroscopy chamber was 1 nTorr. XPS peak areas of Pb(4f) and Te(3d) were measured following a standard Shirley background subtraction. Binding energies were calibrated using the C(1s) peak of adventitious carbon set at 284.8 eV as a reference.[50] The spectra were fitted with software XPS-Peak 4.1. The sample of PbTe nanowires was quickly transferred to the vacuum chamber (within 1 min) after synthesis for the initial measurement. Afterward, the sample was taken out of chamber for exposure to air periodically until the total exposure time is 24 h.

Electrical Conductivity Measurement. The electrical conductivity of a single nanowire was extracted on the basis of $I-V$ curve measurement (conductance) and wire dimensions known from AFM and SEM measurements. The $I-V$ curve measurements were carried out in air by using four contacts fabricated using the method depicted in Figure 9b. Through the two outer electrodes, a constant current was applied using a Keithley sourcemeter 2400. Simultaneously, a Keithley multimeter 2000 measured the voltage at the two inner electrodes. A Labview program was used to control the measurement and collect data. The conductivity σ was calculated using:

$$\sigma = \frac{dI}{dV}\frac{L}{HW} \tag{3}$$

where dI/dV is the slope of the I *versus* V curve, L is the electrically isolated nanowire length, H is the nanowire height, and W its width.

Acknowledgment. This work was supported by the National Science Foundation (Grant DMR-0654055), the Petroleum Research Fund of the American Chemical Society (Grant 46815-AC10), and the UCI School of Physical Sciences Center for Solar Energy. Travis Kruse is acknowledged for creating Figure 1 and Figure 9a,b. J.C.H. and M.A.B. also acknowledge funding from the DOE Office of Basic Energy Sciences (DE-FG02-96ER45576).

REFERENCES AND NOTES

1. Schwarzl, T.; Heiss, W.; Springholz, G.; Aigle, M.; Pascher, H. 6 μm Vertical Cavity Surface Emitting Laser Based on IV−VI Semiconductor Compounds. *Electron. Lett.* **2000**, *36*, 322–324.
2. Springholz, G.; Schwarzl, T.; Aigle, M.; Pascher, H.; Heiss, W. 4.8 μm Vertical Emitting PbTe Quantum-Well Lasers Based on High-Finesse EuTe/Pb_{1-x} Eu_xTe Microcavities. *Appl. Phys. Lett.* **2000**, *76*, 1807–1809.
3. Dughaish, Z. Lead Telluride as a Thermoelectric Material for Thermoelectric Power Generation. *Physica B* **2002**, *322*, 205–223.
4. Heremans, J.; Thrush, C.; Morelli, D. Thermopower Enhancement in Lead Telluride Nanostructures. *Phys. Rev. B* **2004**, *70*, 115334.
5. Heremans, J.; Thrush, C.; Morelli, D. Thermopower Enhancement in PbTe with Pb Precipitates. *J. Appl. Phys.* **2005**, *98*, 063703.
6. *CRC Handbook of Thermoelectrics from Macro to Nano*; Rowe, D., Ed.; CRC Press: Boca Raton, FL, 2006.
7. Goldsmid, H. J. *Electronic Refrigeration*; Pion: London, 1986.
8. Hicks, L.; Dresselhaus, M. Effect of Quantum-Well Structures on the Thermoelectric Figure of Merit. *Phys. Rev. B* **1993**, *47*, 12727–12731.
9. Hicks, L.; Dresselhaus, M. Thermoelectric Figure of Merit of a One-Dimensional Conductor. *Phys. Rev. B* **1993**, *47*, 16631–16634.
10. Balandin, A.; Wang, K. Significant Decrease of the Lattice Thermal Conductivity Due to Phonon Confinement in a Free-Standing Semiconductor Quantum Well. *Phys. Rev. B* **1998**, *58*, 1544–1549.
11. Balandin, A.; Wang, K. Effect of Phonon Confinement on the Thermoelectric Figure of Merit of Quantum Wells. *J. Appl. Phys.* **1998**, *84*, 6149–6153.
12. Walkauskas, S.; Broido, D.; Kempa, K.; Reinecke, T. Lattice Thermal Conductivity of Wires. *J. Appl. Phys.* **1999**, *85*, 2579–2582.
13. Zou, J.; Balandin, A. Phonon Heat Conduction in a Semiconductor Nanowire. *J. Appl. Phys.* **2001**, *89*, 2932–2938.
14. Liu, W.; Cai, W.; Yao, L. Electrochemical Deposition of Well-Ordered Single-Crystal PbTe Nanowire Arrays. *Chem. Lett.* **2007**, *36*, 1362–1363.
15. Fardy, M.; Hochbaum, A. I.; Goldberger, J.; Zhang, M. M.; Yang, P. Synthesis and Thermoelectrical Characterization of Lead Chalcogenide Nanowires. *Adv. Mater.* **2007**, *19*, 3047–3451.
16. Saloniemi, H.; Kanniainen, T.; Ritala, M.; Leskela, M. Electrodeposition of PbTe Thin Films. *Thin Solid Films* **1998**, *326*, 78–82.
17. Saloniemi, H.; Kemell, M.; Ritala, P.; Leskela, M. PbTe Electrodeposition Studied by Combined Electrochemical Quartz Crystal Microbalance and Cyclic Voltammetry. *J. Electroanal. Chem.* **2000**, *482*, 139–148.
18. Zhang, L.; Yu, J.; Mo, M.; Wu, L.; Kwong, K.; Li, Q. A General *In Situ* Hydrothermal Rolling-Up Formation of One-Dimensional, Single-Crystalline Lead Telluride Nanostructures. *Small* **2005**, *1*, 349–354.
19. Sima, M.; Enculescu, I.; Vasile, E. Growth of ZnO Micro and Nanowires Using the Template Method. *J. Optoelectron. Adv. Mater.* **2006**, *8*, 825–828.
20. Tong, H.; Zhu, Y.-J.; Yang, L.-X.; Li, L.; Zhang, L. Lead Chalcogenide Nanotubes Synthesized by Biomolecule-Assisted Self-Assembly of Nanocrystals at Room Temperature. *Angew. Chem., Int. Ed.* **2006**, *45*, 7739–7742.
21. Li, G.-R.; Yao, C.-Z.; Lu, X.-H.; Zheng, F.-L.; Feng, Z.-P.; Yu, X.-L.; Su, C.-Y.; Tong, Y.-X. Facile and Efficient Electrochemical Synthesis of PbTe Dendritic Structures. *Chem. Mater.* **2008**, *20*, 3306–3314.
22. Mokari, T.; Zhang, M.; Yang, P. Shape, Size, and Assembly Control of PbTe Nanocrystals. *J. Am. Chem. Soc.* **2007**, *129*, 9864–9865.
23. Mokari, T.; Habas, S. E.; Zhang, M.; Yang, P. Synthesis of Lead Chalcogenide Alloy and Core−Shell Nanowires. *Angew. Chem., Int. Ed.* **2008**, *47*, 5605–5608.
24. Harman, T.; Taylor, P.; Spears, D.; Walsh, M. Thermoelectric Quantum-Dot Superlattices with High ZT. *J. Electron. Mater.* **2000**, *29*, L1–L4.
25. Harman, T.; Taylor, P.; Walsh, M.; LaForge, B. Quantum Dot Superlattice Thermoelectric Materials and Devices. *Science* **2002**, *297*, 2229–2232.
26. Kungumadevi, L.; Rajasekar, K.; Subbarayan, A.; Sathyamoorthy, R. Structural and DC Conduction Studies on PbTe Thin Films. *Ionics* **2008**, *14*, 63–67.
27. Zhang, G.; Lu, X.; Wang, W.; Li, X. Facile Synthesis of a Hierarchical PbTe Flower-like Nanostructure and Its Shape Evolution Process Guided by a Kinetically Controlled Regime. *Chem. Mater.* **2007**, *19*, 5207–5209.
28. Purkayastha, A.; Yan, Q.; Gandhi, D. D.; Li, H.; Pattanaik, G.; Borca-Tasciuc, T.; Ravishankar, N.; Ramanath, G. Sequential Organic−Inorganic Templating and Thermoelectric Properties of High-Aspect-Ratio Single-Crystal Lead Telluride Nanorods. *Chem. Mater.* **2008**, *20*, 4791–4793.
29. Qiu, X.; Lou, Y.; Samia, A.; Devadoss, A.; Burgess, J.; Dayal, S.; Burda, C. PbTe Nanorods by Sonoelectrochemistry. *Angew. Chem., Int. Ed.* **2005**, *44*, 5855–5857.
30. Tai, G.; Guo, W.; Zhang, Z. Hydrothermal Synthesis and Thermoelectric Transport Properties of Uniform Single-Crystalline Pearl-Necklace-Shaped PbTe Nanowires. *Cryst. Growth Des.* **2008**, *8*, 2906–2911.
31. Tai, G.; Zhou, B.; Guo, W. Structural Characterization and Thermoelectric Transport Properties of Uniform Single-Crystalline Lead Telluride Nanowires. *J. Phys. Chem. C* **2008**, *112*, 11314–11318.
32. Menke, E. J.; Thompson, M. A.; Xiang, C.; Yang, L. C.; Penner, R. M. Lithographically Patterned Nanowire Electrodeposition. *Nat. Mater.* **2006**, *5*, 914–919.
33. Xiang, C.; Kung, S.; Taggart, D.; Yang, F.; Thompson, M.; Gueell, A.; Yang, Y.; Penner, R. Lithographically Patterned Nanowire Electrodeposition: A Method for Patterning Electrically Continuous Metal Nanowires on Dielectrics. *ACS Nano* **2008**, *2*, 1939–1949.
34. Xiang, C.; Yang, Y.; Penner, R. M. Cheating the Diffraction Limit: Electrodeposited Nanowires Patterned by Photolithography. *Chem. Commun.* **2009**, 859–873.
35. Xiang, C.; Guell, A. G.; Brown, M. A.; Kim, J. Y.; Hemminger, J. C.; Penner, R. M. Coupled Electrooxidation and Electrical Conduction in a Single Gold Nanowire. *Nano Lett.* **2008**, *8*, 3017–3022.
36. Yang, F.; Taggart, D. K.; Penner, R. M. Fast, Sensitive Hydrogen Gas Detection Using Single Palladium Nanowires That Resist Fracture. *Nano Lett.* **2009**, *9*, 2177–2182.
37. Yang, Y.; Kung, S. C.; Taggart, D. K.; Xiang, C.; Yang, F.; Brown, M. A.; Guell, A. G.; Kruse, T. J.; Hemminger, J. C.; Penner, R. M. Synthesis of PbTe Nanowire Arrays Using Lithographically Patterned Nanowire Electrodeposition. *Nano Lett.* **2008**, *8*, 2447–2451.
38. Menke, E.; Li, Q.; Penner, R. Bismuth Telluride (Bi_2Te_3) Nanowires Synthesized by Cyclic Electrodeposition/Stripping Coupled with Step Edge Decoration. *Nano Lett.* **2004**, *4*, 2009–2014.
39. Martin-Gonzalez, M.; Prieto, A.; Gronsky, R.; Sands, T.; Stacy, A. High-Density 40 nm Diameter Sb-Rich $Bi_{2-x}Sb_xTe_3$ Nanowire Arrays. *Adv. Mater.* **2003**, *15*, 1003–1006.
40. Martin-Gonzalez, M.; Snyder, G.; Prieto, A.; Gronsky, R.; Sands, T.; Stacy, A. Direct Electrodeposition of Highly Dense 50 nm $Bi_2Te_{3-y}Se_y$ Nanowire Arrays. *Nano Lett.* **2003**, *3*, 973–977.
41. Martin-Gonzalez, M.; Prieto, A.; Gronsky, R.; Sands, T.; Stacy, A. Insights into the Electrodeposition of Bi_2Te_3. *J. Electrochem. Soc.* **2002**, *149*, C546–C554.
42. Prieto, A.; Sander, M.; Martin-Gonzalez, M.; Gronsky, R.; Sands, T.; Stacy, A. Electrodeposition of Ordered Bi_2Te_3 Nanowire Arrays. *J. Am. Chem. Soc.* **2001**, *123*, 7160–7161.
43. Magri, P.; Boulanger, C.; Lecuire, J. Synthesis, Properties and Performances of Electrodeposited Bismuth Telluride Films. *J. Mater. Chem.* **1996**, *6*, 773–779.
44. Kressin, A.; Doan, V.; Klein, J.; Sailor, M. Synthesis of Stoichiometric Cadmium Selenide Films *via* Sequential

Monolayer Electrodeposition. *Chem. Mater.* **1991**, *3*, 1015–1020.
45. Li, Q.; Brown, M. A.; Hemminger, J. C.; Penner, R. M. Luminescent Polycrystalline Cadmium Selenide Nanowires Synthesized by Cyclic Electrodeposition/Stripping Coupled with Step Edge Decoration. *Chem. Mater.* **2006**, *18*, 3432–3441.
46. Menke, E. J.; Brown, M. A.; Li, Q.; Hemminger, J. C.; Penner, R. M. Bismuth Telluride (Bi_2Te_3) Nanowires: Synthesis by Cyclic Electrodeposition/Stripping, Thinning by Electrooxidation, and Electrical Power Generation. *Langmuir* **2006**, *22*, 10564–10574.
47. Patterson, A. The Scherrer Formula for X-ray Particle Size Determination. *Phys. Rev.* **1939**, *56*, 978–982.
48. Marra, W.; Eisenberger, P.; Cho, A. X-ray Total-External-Reflection-Bragg Diffraction-Structural Study of the GaAs-Al Interface. *J. Appl. Phys.* **1979**, *50*, 6927–6933.
49. Bontempi, E.; Colombi, P.; Depero, L.; Cartechini, L.; Presciutti, F.; Brunetti, B.; Sgamellotti, A. Glancing-Incidence X-ray Diffraction of Ag Nanoparticles in Gold Lustre Decoration of Italian Renaissance Pottery. *Appl. Phys. A: Mater. Sci. Process.* **2006**, *83*, 543–546.
50. Wagner, C.; Naumkin, A.; Kraut-Vass, A.; Allison, J.; Powell, C.; Rumble, J. J. *NIST X-ray Photoelectron Spectroscopy Database*; http://srdata.nist.gov/xps/.
51. Bando, H.; Koizumi, K.; Oikawa, Y.; Daikohara, K.; Kulbachinskii, V.; Ozaki, H. The Time-Dependent Process of Oxidation of the Surface of Bi_2Te_3 Studied by X-ray Photoelectron Spectroscopy. *J. Phys.: Condens. Mater.* **2000**, *12*, 5607–5616.
52. Taylor, J.; Perry, D. An X-ray Photoelectron and Electron-Energy Loss Study of the Oxidation of Lead. *J. Vac. Sci. Technol., A* **1984**, *2*, 771–774.
53. Green, M.; Lee, M. Interaction of Oxygen with Clean Lead Telluride Surfaces. *J. Phys. Chem. Solids* **1966**, *27*, 797–804.
54. Yashina, L.; Tikhonov, E.; Neudachina, V.; Zyubina, T.; Chaika, A.; Shtanov, V.; Kobeleva, S.; Dobrovolsky, Y. The Oxidation of PbTe(100) Surface in Dry Oxygen. *Surf. Interface Anal.* **2004**, *36*, 993–996.
55. Rogacheva, E.; Krivulkin, I.; Nashchekina, O.; Sipatov, A.; Volobuev, V.; Dresselhaus, M. Effect of Oxidation on the Thermoelectric Properties of PbTe and PbS Epitaxial Films. *Appl. Phys. Lett.* **2001**, *78*, 1661–1663.
56. Lide, D. *CRC Handbook of Chemistry and Physics*, 88th ed.; CRC Press Taylor and Francis Group: New York, 2007−2008.
57. Moudler, J.; Stickle, W.; Sobol, P.; Bomben, K. *Handbook of X-ray Photoelectron Spectroscopy*; Perkin-Elmer, Physical Electronics Division: Eden Prarie, MN, 1992.
58. Peng, Z.; Peng, X. Mechanisms of the Shape Evolution of CdSe Nanocrystals. *J. Am. Chem. Soc.* **2001**, *123*, 1389–1395.
59. Powell, C. J.; Jablonski, A. *NIST Electron Inelastic-Mean-Free-Path Database*, version 1.1; National Institute of Standards and Technology: Washington, DC, 2000.
60. Rogacheva, E.; Lyubchenkoa, S.; Dresselhaus, M. Effect of Oxidation on Thickness Dependencies of Thermoelectric Properties in PbTe/Mica Thin Films. *Thin Solid Films* **2005**, *476*, 391–395.